Article

# Electrochemical Templating of Metal Nanoparticles and Nanowires on Single-Walled Carbon Nanotube Networks

Thomas M. Day, Patrick R. Unwin, Neil R. Wilson, and Julie V. Macpherson

*J. Am. Chem. Soc.*, **2005**, 127 (30), 10639-10647• DOI: 10.1021/ja051320r • Publication Date (Web): 12 July 2005



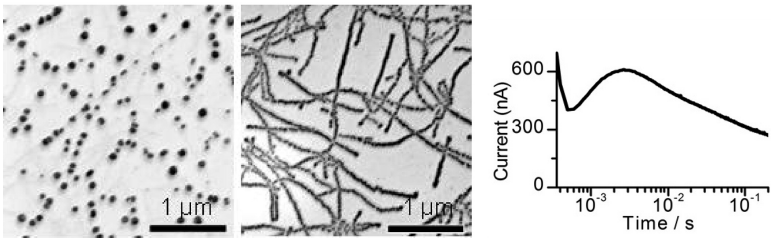


## More About This Article

Additional resources and features associated with this article are available within the HTML version:

- Supporting Information
- Links to the 24 articles that cite this article, as of the time of this article download
- Access to high resolution figures
- Links to articles and content related to this article
- Copyright permission to reproduce figures and/or text from this article

View the Full Text HTML

J|A|C|S
ARTICLES
Published on Web 07/12/2005

# Electrochemical Templating of Metal Nanoparticles and Nanowires on Single-Walled Carbon Nanotube Networks

Thomas M. Day,[†] Patrick R. Unwin,[†] Neil R. Wilson,[‡] and Julie V. Macpherson*,[†]

*Contribution from the Departments of Chemistry and Physics, University of Warwick, Coventry CV4 7AL, United Kingdom*

Received March 2, 2005; E-mail: j.macpherson@warwick.ac.uk

***Abstract:*** The use of single-walled carbon nanotube (SWNT) networks as templates for the electrodeposition of metal (Ag and Pt) nanostructures is described. Pristine SWNTs, grown on insulating $SiO_2$ surfaces using catalyzed chemical vapor deposition, served as the working electrode. In the simplest case, electrical contact was made by depositing a gold strip on the SWNT substrate (device 1). Deposition of Ag and Pt over extensive periods (30 s) resulted in a high density of particles on the SWNTs, with almost contiguous nanowire formation from the Au/SWNT boundary moving to isolated nanoparticles at further distances from the contact. For direct electrochemical studies of Ag and Pt nucleation, the assembly was coated in a resist layer and a small window opened up to expose only the electrically connected SWNTs to solution (device 2). In this case, the electrochemical signature in voltammetric and amperometric studies of metal deposition was due solely to processes at the SWNTs. Coupled with high-resolution microscopy measurements (atomic force microscopy and field emission scanning electron microscopy), this approach provided detail on the nucleation and growth mechanisms of Ag and Pt on SWNTs under electrochemical control. In particular, Ag growth was found to be rapid and progressive with an increasing nanoparticle density with time, whereas Pt deposition was characterized by lower nucleation densities and slower growth rates with a tendency for larger particles to be produced over long times.

## Introduction

The development of methods for producing metallic and semiconducting nanowires and nanoparticles of defined, uniform size is a key theme in nanoscience research. When the characteristic dimension of a nanostructure reaches a critical size, interesting chemical and physical properties are revealed,[1] such as novel luminescent characteristics[2] and quantized electron-transfer events.[3] There are now a myriad of fabrication procedures for the synthesis of nanoparticles and nanowires, many of which are based on solution-phase chemical processes.[4]

Electrodeposition is proving an increasingly attractive route for the preparation of nanostructured materials when used with appropriate templates. For example, mesoporous membranes, with defined monodisperse pores, can serve as templates for the electrodeposition of a metal from a solution of its salt. In this way, Au, Pt, Ag, Ni, Cu, Co, and ZnO wires with diameters in the range 10−500 nm have been deposited[5,6] in membranes such as track-etched polycarbonate and porous aluminum oxide. Using an alternative approach, Penner and co-workers[7] have demonstrated that metal nanostructures can be deposited at particular sites on low-energy surfaces (such as basal plane graphite) rather than grow via a layer-by-layer mechanism. Careful control of the electrodeposition parameters allowed selection between the growth of nanoparticles (largely on terraces) and that of nanowires (templated along step edges).[7−10]

There has been recent interest in the use of single-walled carbon nanotubes (SWNTs) as templates for the formation of nanoparticles and nanowires. SWNTs essentially consist of a graphene sheet folded to produce a cylindrical structure ca. 1 nm in diameter and display unique mechanical and electrical properties.[11] Composite structures containing SWNTs coated in a metal to form either nanoparticles or nanowires have shown particular promise as chemical sensors.[12,13] It has also been demonstrated that the combination of Pt nanoparticles with SWNTs produces interesting electrode materials for catalytic applications[14] and electrochemical biosensing.[15]

[†] Department of Chemistry.
[‡] Department of Physics.

(1) Schmid, G. *Chem. Rev.* **1992**, *92*, 1709.
(2) Alivisatos, P. *Nat. Biotechnol.* **2004**, *22*, 47.
(3) Schmid, G.; Simon, U. *Chem. Commun.* **2005**, 697.
(4) See for example: Kamat, P. V. *J. Phys. Chem. B* **2002**, *106*, 7729 and references therein.
(5) Bauer, L. A.; Birenbaum, N. S.; Meyer, G. J. *J. Mater. Chem.* **2004**, *14*, 517.
(6) See, for example: (a) Martin, C. R. *Science* **1994**, *266*, 1961. (b) Miller, S. A.; Young, V. Y.; Martin, C. R. *J. Am. Chem. Soc.* **2001**, *123*, 12355. (c) Schönenberger, C.; van der Zande, B. M. I.; Fokkink, L. G. J.; Henny, M.; Schmid, C.; Krüger, M.; Bachtold, A.; Huber, R.; Birk, H.; Staufer, U. *J. Phys. Chem. B* **1997**, *101*, 5497. (d) Tian, M.; Wang, J.; Kurtz, J.; Mallouk, T. E.; Chan, M. H. W. *Nano Lett.* **2003**, *3*, 919. (e) Thurn-Albrecht, T.; Schotter, J.; Kästle, G. A.; Emley, N.; Shibauchi, T.; Krusin-Elbaum, L.; Guarini, K.; Black, C. T.; Tuominen, M. T.; Russell, T. P. *Science* **2000**, *290*, 2126.
(7) Penner, R. M. *J. Phys. Chem. B* **2002**, *106*, 3339.
(8) Liu, H.; Penner, R. M. *J. Phys. Chem. B* **2000**, *104*, 9131.
(9) Favier, F.; Walter, E.; Zach, M. P.; Benter, T.; Penner, R. M. *Science* **2001**, *293*, 2227.
(10) Walter, E. C.; Zach, M. P.; Favier, F.; Murray, B. J.; Inazu, K.; Hemminger, J. C.; Penner, R. M. *ChemPhysChem* **2003**, *4*, 131.
(11) Saito, R.; Dresselhaus, G.; Dresselhaus, M. S. *Physical Properties of Carbon Nanotubes*; Imperial College Press: London, 1998.
(12) Bezryadin, A.; Lau, C. N.; Tinkham, M. *Nature* **2000**, *404*, 971.
(13) Kong, J.; Chapline, M. G.; Dai, H. *Adv. Mater.* **2001**, *13*, 1384.

10.1021/ja051320r CCC: $30.25 

Nanostructure−SWNT composite structures have been formed in several ways. The metal of interest can be directly deposited onto the SWNT using either sputtering or thermal evaporation techniques,[12,13,16] or added as preformed nanoparticles to a solubilized solution of SWNTs.[15] Alternatively, by oxidatively functionalizing the side walls and ends of an SWNT, metal nanoparticles can be covalently tethered (via linker molecules) to oxidized defect sites in the SWNT.[17] Dai and colleagues reported that for certain metal salt solutions (e.g., $PtCl_4^{2-}$, $AuCl_4^-$ in a water/ethanol mix) metal deposition occurred spontaneously due to direct redox reactions between the metal ions and SWNTs (electroless metal deposition).[18] For example, Pt and Au were found to deposit as nanoparticles along the sidewall of SWNTs, which grew in size with time.

The use of electrolysis offers an attractive means of controlling the nucleation and growth of metals. With careful choice of substrate, deposition potential, and growth time, it is possible to direct the process toward either nanoparticle or nanowire growth, with a high degree of monodispersity in particle size.[7−10] Moreover, analysis of the resulting current−time behavior, together with microscopy characterization, provides considerable information on the growth mechanism. In contrast to many macroscopic planar surfaces, the 1D nature of SWNTs makes this a particularly attractive template for metal electrodeposition, since it offers the possibility of size and directional control of the growth process.

Direct electrodeposition has recently been reported for the formation of nanoparticle−SWNT composites.[14,19] However, in neither case was the growth mechanism studied in detail. In this paper we demonstrate, using Ag and Pt, that *both* metal nanoparticles and nanowires can be grown on pristine SWNT networks under electrochemical control and present an examination of the nucleation and growth processes involved. As in our recent voltammetric studies with networks of SWNTs on insulating surfaces,[20] the SWNTs are electrically connected to a Au contact electrode, which is electrically isolated from solution so that, when required, electrochemical signatures can be attributed solely to the processes occurring at SWNTs.[20,21] Potential step chronoamperometric measurements coupled with high-resolution microscopy studies are shown to provide an insight into the nucleation and growth mechanism of metal particles on SWNTs and highlight differences in the kinetics and mechanisms of Pt and Ag deposition.

## Experimental Methods

**SWNT Synthesis.** SWNTs were grown on $Si/SiO_2$ substrates (300 nm of thermally grown $SiO_2$) by catalyzed chemical vapor deposition (cCVD), using iron nanoparticles (ferric nitrate nonahydrate, Aldrich Chemicals) as the catalyst.[22,23] The substrates were placed in a 1 in. tube furnace and annealed under a flow of $H_2$, 500 standard cubic centimeters per minute (sccm) at 950 °C for 10 min. $CH_4$ (as the carbon-containing gas) was then added at 1500 sccm for a further 10 min. SWNT diameters were determined by atomic force microscopy (AFM) and found to be in the range 1−3 nm. SWNT densities were determined by measuring the total length of SWNTs present per unit area of substrate ($\mu m_{SWNT}\ \mu m^{-2}$) using AFM and field emission scanning electron microscopy (FE-SEM). All studies focused on high-density networks of pristine SWNTs (where the percolation threshold was exceeded[20,24]). The SWNT network density was typically ~5 $\mu m_{SWNT}\ \mu m^{-2}$, with specific densities quoted throughout the paper. At these high densities it is difficult to measure the length of the individual SWNTs present; however, samples containing a low density of SWNTs (approximately one SWNT per 10 $\mu$m × 10 $\mu$m area of substrate) showed a wide range of lengths from ~1−100 $\mu$m with a median value of ~10 $\mu$m.

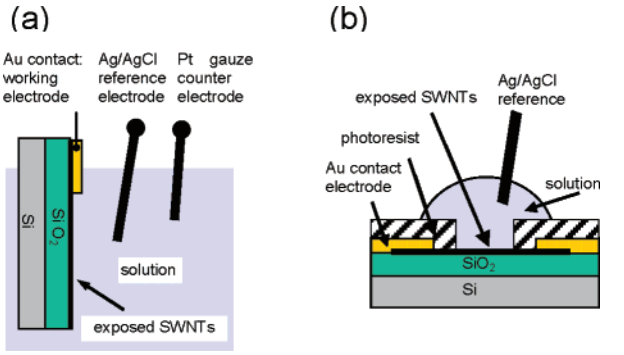


***Figure 1.*** Schematics of the setups used for (a) working electrode device 1, which consists of a Au band, 200 $\mu$m in width, ca. 4 mm long connected to a network of pristine SWNTs, and (b) working electrode device 2. In the latter case, the electrode is a 20 $\mu$m × 400 $\mu$m area of high-density SWNTs, with the electrical contact insulated from the solution using a resist.

**SWNT Electrode Fabrication.** Two types of working electrodes were employed. In device type 1, shown schematically in Figure 1a, a contact electrode (60 nm of Au with a 10 nm Cr adhesive layer) of width 200 $\mu$m and length ca. 4 mm was thermally evaporated across one edge of an SWNT substrate. The procedure for fabricating device type 2 (Figure 1b) is described in detail elsewhere.[20] In brief, Cr/Au (10 nm/60 nm) contact electrodes were thermally evaporated onto the SWNT substrates, through a copper mask, to produce two Au band electrodes separated by a gap 90 $\mu$m wide by 1 mm long. A 1.5 $\mu$m layer of photoresist (Microposit S1818, Rohm and Haas Electronic Materials) was then spin coated onto the substrate to insulate the whole surface. Using a confocal microscope (Zeiss LSM 510), a 400 $\mu$m by 20 $\mu$m area of the resist was lithographically exposed between the two insulated Au electrodes, and subsequently removed, to leave an exposed area of electrically connected SWNTs. FE-SEM evidence of photoresist residue, which caused subsequent metal growth to be confined to specific areas of the exposed area, was only found on a limited number of substrates. These samples were discarded.

**Solutions.** All aqueous solutions were prepared using Milli-Q reagent water (Millipore Corp.). Silver deposition solutions usually contained 1 mM silver nitrate (99+%, Aldrich Chemicals) with 0.2 M potassium nitrate (Analytical Grade, Fisher Scientific) as the supporting electrolyte. Platinum deposition solutions usually contained 2 mM potassium hexachloroplatinate (Sigma-Aldrich) with 0.5 M perchloric acid acting as a supporting electrolyte.[25]

(14) Girishkumar, G.; Vinodgopal, K.; Kamat, V. *J. Phys. Chem. B* **2004**, *108*, 19960.
(15) Hrapovic, S.; Liu, Y.; Male, K. B.; Luong, J. H. T. *Anal. Chem.* **2004**, *76*, 1083.
(16) Zhang, Y.; Dai, H. *Appl. Phys. Lett.* **2000**, *77*, 3015.
(17) Azamian, A.; Coleman, K. S.; Davis, J. J.; Hanson, N.; Green, M. L. *Chem. Commun.* **2002**, 366.
(18) Choi, H. C.; Shim, M.; Bangsaruntip, S.; Dai, H. *J. Am. Chem. Soc.* **2002**, *124*, 9058.
(19) After submission of our work for publication, the following paper was published: Quinn, B. M.; Dekker: C.; Lemay, S. G. *J. Am. Chem. Soc.* **2005**, *127*, 6146.
(20) Day, T. M.; Wilson, N. R.; Macpherson, J. V. *J. Am. Chem. Soc.* **2004**, *126*, 16724.
(21) Heller, I.; Kong, J.; Heering, H. A.; Williams, K. A.; Lemay, S. G.; Deeker, C. *Nano Lett.* **2005**, *5*, 137.
(22) Hafner, J. H.; Cheung, C. L.; Oosterkamp, T. H.; Lieber, C. M. *J. Phys. Chem. B* **2001**, *105*, 743.
(23) Wilson, N. R.; Cobden, D. H.; Macpherson, J. V. *J. Phys. Chem. B* **2002**, *106*, 13102.
(24) Snow, E. S.; Novak, J. P.; Campbell, P. M.; Park, D. *Appl. Phys. Lett.* **2003**, *82*, 2145.
(25) Stoychev, D.; Papoutsis, A.; Kelaidopoulou, A.; Kokkinidis, G.; Milchev, A. *Mater. Chem. Phys.* **2001**, *72*, 360.

**Procedures.** Current−voltage (cyclic voltammetry (CV)) and current−time (chronoamperometry) measurements were carried out in either a two- or three-electrode mode using a commercial potentiostat (CH750A Electrochemical Workstation, CH Instruments). The electrodeposition of Ag and Pt onto device 1 was conducted by immersing the substrate into solution so that part of the gold band and electrically connected SWNTs (ca. 2/3 of the overall substrate area) were placed in the solution. This served as the working electrode, and a Ag/AgCl wire and Pt gauze functioned as the reference and counter electrodes, respectively. Experiments using device 2 employed a droplet cell setup,[20] in a two-electrode mode, where the electrically connected SWNTs served as the working electrode and a Ag/AgCl wire acted as the reference electrode. For both electrode devices a variety of experiments were carried out to investigate the effect of deposition potential and deposition time on the metal nucleation characteristics.

**Characterization.** The deposited metal structures were analyzed using both AFM and FE-SEM. FE-SEM images were taken using a SUPRA 55 VP FE-SEM instrument (Zeiss). Prior to imaging, the samples were removed from solution and rinsed very carefully with water. AFM images were acquired in tapping mode using a Veeco Multimode AFM instrument with a Nanoscope IIIa controller and an Extender module. During AFM imaging of the deposited Ag nanoparticles, streaking was occasionally observed, especially in the images recorded at higher tip velocities ($>10\ \mu m\ s^{-1}$), corresponding to higher tip sample forces. Subsequent inspection of the AFM tip by TEM revealed particles at the tip apex, which were confirmed to be Ag by X-ray analysis. This indicated that the AFM tip was moving some Ag nanoparticles while imaging, and indeed, some were deposited onto the tip itself. By contrast, the Pt nanoparticles appeared to be stable and were not moved or removed by the tip. All the AFM images and analyses presented here were taken at low enough scan rates for the imaging to be noninvasive, allowing an accurate representation of nanoparticle sizes and densities.

For electric force microscopy (EFM) measurements the tips were highly doped Si, resonance frequency ~80 kHz and spring constant ~0.6 N $m^{-1}$ (MikroMasch). Two contact electrodes were deposited onto a typical SWNT sample by Au evaporation (with a Cr adhesive layer) through a copper mask, forming a pair of electrodes separated by a gap of ~25 $\mu$m (1 mm length). EFM imaging was performed in "lift mode", where the AFM tip scans each line first in tapping mode and then retraces it a set distance, here 100 nm, above the surface. While the tip was lifted off the surface, a bias voltage was applied to the right-hand electrode, with both the tip and left-hand electrode grounded. A potential difference, $V_{ts}$, between the tip and the surface beneath it causes a change in the phase of oscillation of the tip proportional to $V_{ts}^2$, which can then be recorded to give a map of the local potential on the sample.[26]

## Results and Discussion

**Potential Distribution in High-Density SWNT Networks.** For all experiments high-density SWNT networks were employed to ensure good electrical connectivity over large distances. To obtain quantitative information on the electrical connectivity of the network, prior to electrochemically controlled metal deposition, the potential drop across the high-density SWNT networks was investigated using EFM. Figure 2a shows a tapping mode height image of a region between the two Au contact electrodes, both of which are just visible on the left and right sides of the image. Figure 2b is the simultaneously acquired EFM image, recorded with the left-hand electrode grounded and an applied bias of −2 V to the right-hand electrode.

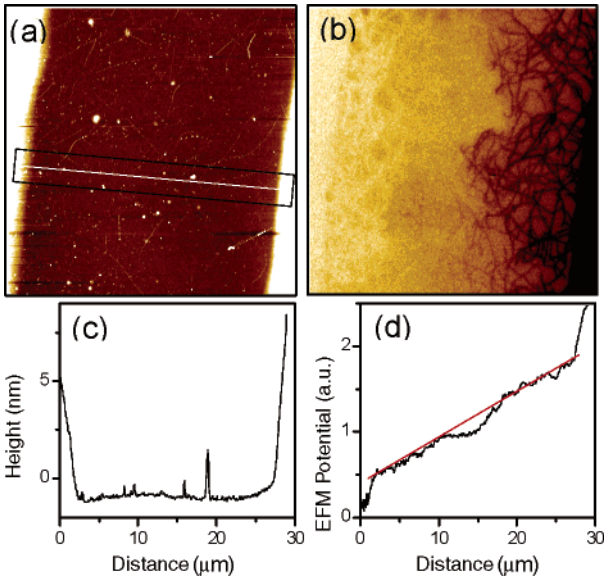


***Figure 2.*** (a) Topography and (b) simultaneously captured dc-EFM image of a network of SWNTs between two Au contacts placed 25 $\mu$m apart. (c) and (d) are cross-sectional line scans averaged over the box indicated in (a). The applied bias was −2 V (to the right-hand electrode), and the dc-EFM image was taken at a lift height of 100 nm. The red line in (d) highlights the effectively linear potential drop across the network of SWNTs.

The network of SWNTs is evident in the EFM image; it is also clear that the SWNTs are electrically connected both to each other and to the contact electrodes. Figure 2c is the height line scan over the box marked in Figure 2a, while Figure 2d is the EFM line scan from the corresponding region in Figure 2b (not marked). The EFM data in Figure 2d have been adjusted so that they are directly proportional to $V_{ts}$.[27] In the region between the two contact electrodes (a separation distance of ca. 25 $\mu$m) the potential drop across the SWNT network is predominantly linear, as shown by the red line (added as a guide to the eye), and hence, the SWNT density is well above the percolation threshold. The small variation in the linear potential profile reflects the random nature of the network. At the two Au contact electrodes the potential gradient rises more steeply (reaching a plateau at further distances out, but not shown here) due to the nature of the SWNT−Au contact resistance. For this high-density sample (typical of those employed in all studies described herein) the EFM data show[28] that just less than half the potential is dropped at the contacts between the SWNT and the metal electrodes, with the remainder being dropped along the SWNTs and at the SWNT to SWNT contacts.

This result demonstrates that high-density SWNT networks are conductive, and hence should be electrochemically active at relatively long distance from the contact electrodes, although the extent will also depend on the kinetics of the metal deposition process. The linear potential drop indicates that at high density the SWNTs act electrically as a conducting 2D layer for which a 2D conductivity can be determined. The resistance between the two electrodes in this sample was measured to be ~3 kΩ. Given that about half of this value is

(26) Gil, A.; Colchero, J.; Gómez-Herrero, J.; Baró, A. M. *Nanotechnology* **2003**, *14*, 332.

(27) A constant phase was subtracted, and the square root of the resultant phase difference was then found.

(28) The proportional drop in potential will depend on the separation between the electrodes and the density of the SWNTs. The conductivity of the SWNT network decreases with decreasing SWNT density. However, in this case the linear drop in potential shows that the network is well above the percolation threshold.

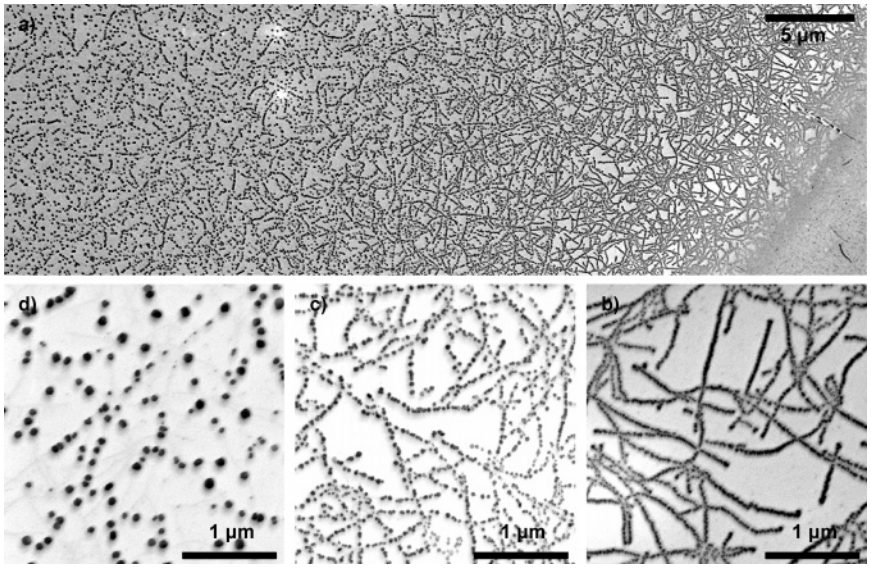


***Figure 3.*** FE-SEM images showing (a) Ag deposited on SWNTs, using electrode device 1, from a solution containing 1 mM $AgNO_3$ in 0.2 M $KNO_3$. A deposition potential and time of −0.4 V (versus Ag/AgCl) and 30 s were used. The SWNT network density was 6.1 $\mu m_{SWNT}$ $\mu m^{-2}$. In the bottom right of (a) is the Au contact electrode which was also exposed to solution. (b)−(d) are higher resolution FE-SEM images: (b) close to, (c) ca. 15 $\mu$m from, and (d) further away (ca. 30 $\mu$m) from the contact electrode.

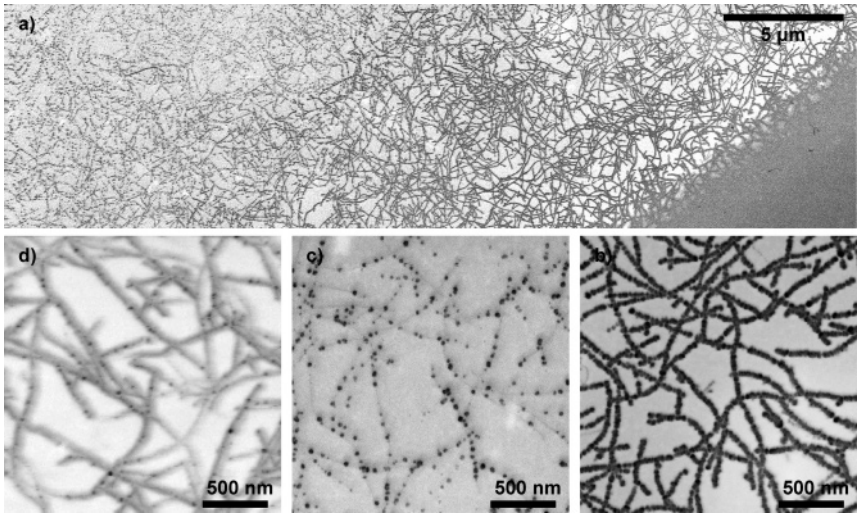


***Figure 4.*** FE-SEM images showing (a) Pt deposited on SWNTs, using electrode device 1, from a solution containing 2 mM $K_2PtCl_6$ in 0.5 M perchloric acid. A deposition potential and time of −0.4 V (versus Ag/AgCl) and 30 s were used. The SWNT network density was 6.8 $\mu m_{SWNT}$ $\mu m^{-2}$. In the bottom right of the image is the Au contact electrode which was also exposed to solution. (b)−(d) are higher resolution FE-SEM images: (b) close to, (c) ca. 15 $\mu$m from, and (d) further away (ca. 25 $\mu$m) from the contact electrode.

due to contact resistance between the Au and SWNTs, we estimate the 2D conductivity of the SWNT networks of the type used for the studies herein to be $\sim 10^{-5}$ S.

**Metal Deposition at Device Type 1: Nanowire and Nanoparticle Formation.** Initial metal deposition studies were morphological, with deposition carried out for a defined period, and high-resolution imaging techniques were used to identify the nucleation characteristics of the deposited material. For these investigations device type 1 was used due to its ease of fabrication; in addition the exposed SWNTs in device 1 were not subject to any postsynthesis processing (such as the photolithography required for device 2). Figures 3 and 4 show FE-SEM images taken after Ag and Pt deposition, respectively. The color has been reversed, compared to that of conventional FE-SEM images, using image analysis software. The metal nanoparticles appear dark gray-black and the insulating $SiO_2$ light gray-white. In both cases, deposition was promoted by stepping the applied potential from a value of 0.0 V (where there was no electrode reaction) to −0.4 V (versus Ag/AgCl) for a period of 30 s and then back to open circuit. It is difficult to set precisely the same driving forces for Ag and Pt electrodeposition, not least because standard electrode potentials relate to macroscopic systems, while the processes here involve nanoparticle formation, for which the standard potentials are size-dependent and differ significantly from those of the bulk.[29]

A deposition potential of −0.4 V was chosen for Ag, as it was just into the limiting current plateau for $Ag^+$ reduction as discerned from CV measurements (vide infra). In the case of Pt, this potential was just below the limiting current plateau deduced from similar measurements. There were some restric-

(29) Plieth, W. J. *J. Phys. Chem.* **1982**, *86*, 3166.

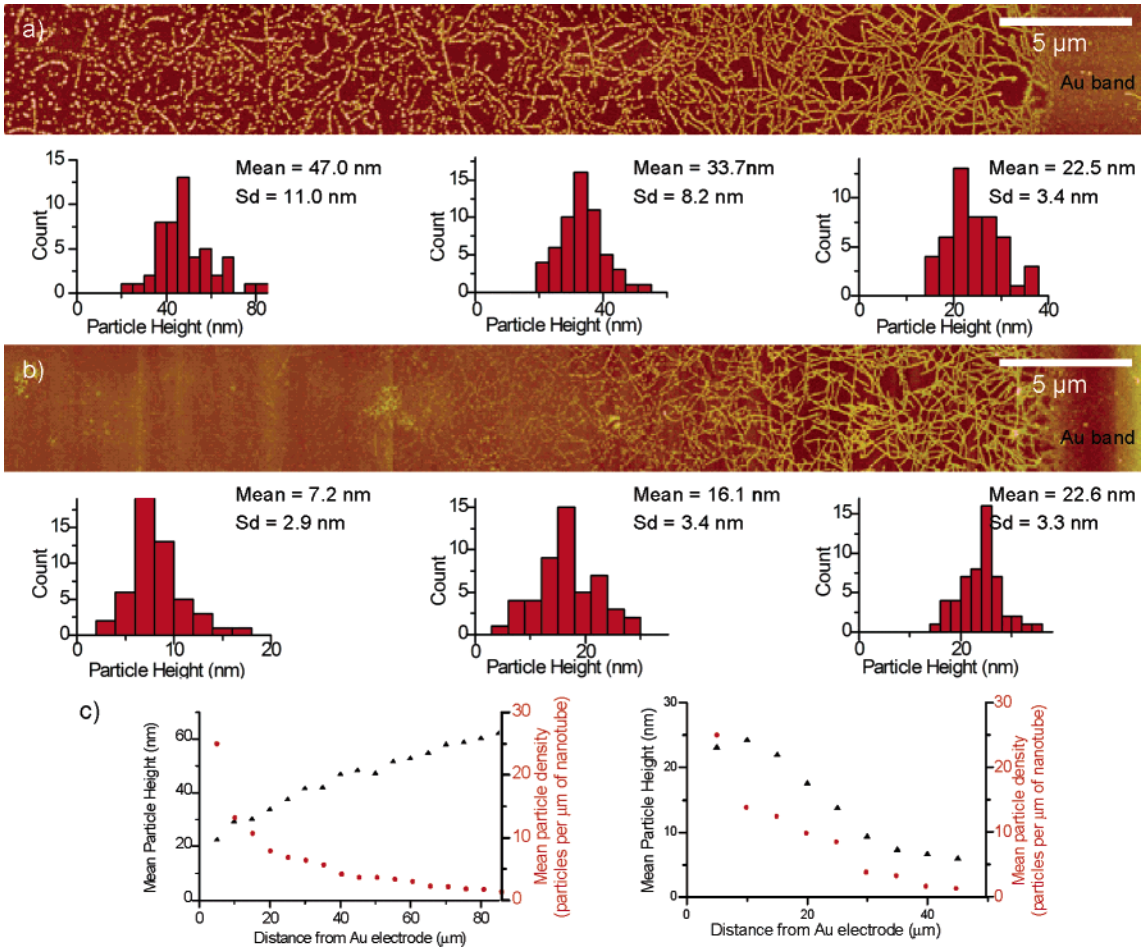


***Figure 5.*** AFM images of the areas shown by FE-SEM in Figures 3 and 4 for (a) Ag deposition and (b) Pt deposition on an SWNT network electrode (device 1). Analysis of particle height in three regions from the Au contact electrode (at distances of 5, 20, and 40 $\mu$m) is shown in the histograms. (c) Mean particle height and particle density as a function of distance from the contact electrode (the left plot is for Ag, and right plot is for Pt). Data were taken from AFM images recorded every 5 $\mu$m from the Au contact electrode.

tions on the cathodic potential range for Pt, due to complications from hydrogen evolution occurring at more negative potentials in the perchloric acid supporting electrolyte solution.

In Figures 3 and 4, apart from the gold contact electrode, metal is only deposited on the SWNT network, as confirmed using AFM. The underlying $SiO_2$ is insulating and so is electrically inert. FE-SEM images were typically recorded at 10 kV to enable the metal particles to be clearly identified, but at the expense of visualizing the SWNTs. FE-SEM imaging of SWNTs is best carried out at lower accelerating voltages, $\leq$1 kV.[30] However, it was sometimes possible to identify both the SWNTs and the metal nanoparticles in the same image (for example, Figures 3d and 4c,d). FE-SEM images of typical metal−SWNT composite structures, recorded at both 1 and 10 kV, are provided in the Supporting Information to further confirm the growth of the metal nanoparticles solely on the SWNT network. Significantly, for both metals, a high density of nanoparticles was deposited close to the gold contact electrode (within a distance of ca. 10 $\mu$m from the edge), tending toward the formation of nearly contiguous nanoparticles or nanowire structures. Further away from the contact, the nanoparticle density decreased and discrete nanoparticles are clearly visible.

AFM was also used to provide a quantitative analysis of particle sizes (Figure 5). In all AFM particle size analyses that follow, heights were measured, rather than widths, to avoid tip convolution effects in the latter. The lateral dimensions of nanoparticles on several different Pt and Ag samples were also measured using FE-SEM: in the majority of cases the lateral dimension determined was only a few nanometers larger than the AFM height, consistent with the nanoparticles present being approximately spherical. The AFM images in Figure 5, recorded as a function of distance from the gold contact (a series of smaller 5 $\mu$m $\times$ 5 $\mu$m scans collated together to form the final image), were obtained in the same area as the FE-SEM images shown in Figures 3 and 4. Analysis of particle height in three regions from the Au contact electrode (at distances of 5, 20, and 40 $\mu$m) is shown in the histograms. Plots of mean particle height and particle density as a function of separation distance from the contact electrode are also shown.

For both metals, close to the contact electrode the nanoparticles merged to form nearly uniform nanowires with heights of ca. 23 $\pm$ 3 nm. The Ag nanoparticles decreased in density away from the electrode, and increased in size. By comparison, the Pt nanoparticles did not extend as far from the contact electrode (80 $\mu$m for Pt compared with 400 $\mu$m for Ag) and decreased both in size and in density with distance from the contact. At 20 $\mu$m from the contact, the particle size was

(30) Brintlinger, T.; Chen, Y.-F.; Dürkop, T.; Cobas, E.; Furher, M. S. *Appl. Phys. Lett.* **2002**, *81*, 2454.

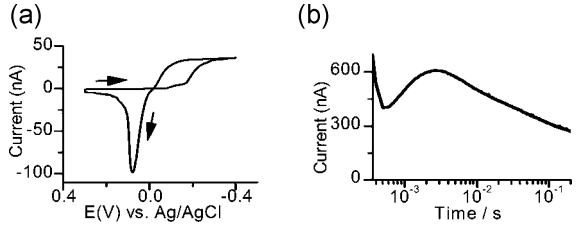


***Figure 6.*** (a) Cyclic voltammogram for the reduction of $Ag^+$ to Ag and subsequent oxidation (stripping) to $Ag^+$ at a SWNT network electrode (SWNT density 3.5 $\mu m_{SWNT}$ $\mu m^{-2}$). The solution contained 1 mM $AgNO_3$ in 0.2 M $KNO_3$, and the potential was swept at a scan rate of 50 mV $s^{-1}$. (b) Current vs time for the electrodeposition of Ag at a high-density SWNT network electrode (SWNT density 4.1 $\mu m_{SWNT}$ $\mu m^{-2}$). The potential of the electrode was stepped from 0.0 to −1.0 V (versus Ag/AgCl) for 200 ms. The solution contained 1 mM $AgNO_3$ in 0.2 M $KNO_3$.

ca. 34 ± 8 nm for Ag compared to 16 ± 3 nm for Pt. At a distance of 40 $\mu$m, the particle size was ca. 47 ± 11 nm for Ag, while it was ca. 7 ± 3 nm for Pt (see the histogram analysis in Figure 5).

These striking results demonstrate that, using this simple approach, both relatively monodisperse particles and nanowires can be formed selectively on SWNTs under electrochemical control. This represents an attractive alternative to the use of sputtering or evaporation techniques for the formation of SWNT-based nanowires. Here, the metal cannot be simply deposited on SWNTs lying on a sample surface, as the entire substrate would be coated in a thin film of the material of interest (for noncontinuous films less than 1 nm thick this approach has been used[13]). Consequently, involved lithographic procedures are required to produce a working device.[12]

The variation in metal particle density (i.e., nanowires close to the Au contact electrode tending to isolated nanoparticles further away) is likely to be due to a decreased driving potential with distance. Although the SWNTs in the network are well-connected (as verified by the data in Figure 2), there will, nonetheless, be a potential gradient in the plane of the network during electrolysis, the nature of which will depend on the current distribution across the network due to the electrodeposition process. The potential distribution will favor metal nucleation closer to the Au electrode, and as particles subsequently deposit and grow in this region, the resulting increase in local current density will tend to further distort the potential distribution. The much longer distance over which Ag nanoparticles are formed is attributed to the higher driving force employed (at the gold contact) for Ag compared with Pt.

**Metal Deposition at Device 2.** To gain further insight into the mechanisms involved in the nucleation of both Ag and Pt nanoparticles at pristine SWNTs, it was necessary to isolate the electrode contacting the SWNTs from the solution; this was achieved using device type 2 (Figure 1b). With this electrode, a well-defined region is exposed to the solution, such that the SWNT network alone constitutes the working electrode. No deposition was observed when the SWNTs were absent from the device. Thus, this approach enabled the analysis of voltammetric and chronoamperometric data, together with microscopy studies on the deposited metal nanostructures.

**1. Ag Deposition.** Figure 6 shows (a) a typical example of a cyclic voltammogram for Ag deposition, recorded on a pristine SWNT electrode (i.e., no prior Ag deposition/stripping waves had been run on the sample) at a scan rate of 50 mV $s^{-1}$, from a starting potential of +0.3 V, and (b) a chronoamperometric response over a period of 200 ms, after the potential of the device was stepped from 0.0 to −1.0 V vs Ag/AgCl to drive the electrodeposition process. The cyclic voltammogram shows the characteristic behavior for electrodeposition, with a cathodic current flowing beyond −0.2 V, reaching a plateau value of ca. 38 nA at −0.4 V. The half-wave potential for this process was ca. 150 mV more cathodic than for the same process on a Au ultramicroelectrode (25 $\mu$m diameter). As the potential scan direction was reversed a characteristic stripping peak for the reoxidation of Ag to $Ag^+$ was observed. A net charge of 6.91 × $10^{-9}$ C was passed on the forward sweep, with a significant proportion of this charge recovered on the reverse sweep.

The chronoamperometric behavior in Figure 6b provides considerable information on the electrodeposition process. Following an initial rapid decay in the charging current, immediately after the potential step, the current attains a value of ca. 400 nA and then increases to 600 nA over a period of ca. 3 ms. This is consistent with the behavior expected for very rapid nucleation and growth of particles, where the active surface area increases sharply. Thereafter, the current decreases with time, which is attributable to the overlap of the diffusion fields of neighboring metal particles. This occurs when particles are within a few particle radii of each other, leading eventually to the development of an extensive (planar) diffusion field across the sample. This latter part of the $i-t$ curve does not have the classical Cottrellian form,[31] but rather an approximate $t^{-1/5}$ current dependence. This is a consequence of the rather complicated nucleation process in this time domain (vide infra) and of the finite size of the exposed SWNT electrode region that results in the current tending toward a quasi steady state.

Figure 7 shows FE-SEM and AFM analysis of several networks, with similar high SWNT densities, after deposition of Ag using potential step chronoamperometry for times of (a) 200 ms, (b) 500 ms, and (c) 3 s, at a deposition potential of −1.0 V. A low-magnification FE-SEM image of Figure 7c showing growth of Ag within the exposed gap is given in the Supporting Information. The density of particles increases with time from 5.2 particles $\mu m^{-1}{}_{SWNT}$ at 200 ms (SWNT density 2.89 $\mu m_{SWNT}$ $\mu m^{-2}$) to 6.9 particles $\mu m^{-1}{}_{SWNT}$ at 500 ms (SWNT density 3.45 $\mu m_{SWNT}$ $\mu m^{-2}$) and 9.6 particles $\mu m^{-1}{}_{SWNT}$ at 3 s (SWNT density 4.91 $\mu m_{SWNT}$ $\mu m^{-2}$). Although the mean particle height remains approximately the same, ca. 28−29 nm, there is a broadening of the size distribution of the particles (see the histogram analysis in Figure 7) and an increase in the mean volume of the nanoparticles with deposition time.

Figure 8 shows typical current−time ($i-t$) plots for deposition of Ag for 500 ms at potentials of −0.1, −0.2, and −1.0 V. At −0.1 V, no cathodic current flows and no particles were detected on the sample by either AFM or FE-SEM. At −0.2 V, particles are formed at a density of 2.8 particles $\mu m^{-1}{}_{SWNT}$ (1.98 $\mu m_{SWNT}$ $\mu m^{-2}$), whereas at −1.0 V this density increased to 4.5 particles $\mu m^{-1}{}_{SWNT}$ (2.30 $\mu m_{SWNT}$ $\mu m^{-2}$). Note, however, that in both cases similar mean particle heights result, ca. 25 ± 1 nm (see the histogram analysis). Thus, for Ag deposition the applied potential appears to largely control the nucleation rate on the SWNT and has little effect on the size of the nanoparticles formed.

(31) Bard, A. J.; Faulkner, L. R. *Electrochemical Methods, Fundamentals and Applications*; Wiley: New York, 1980.

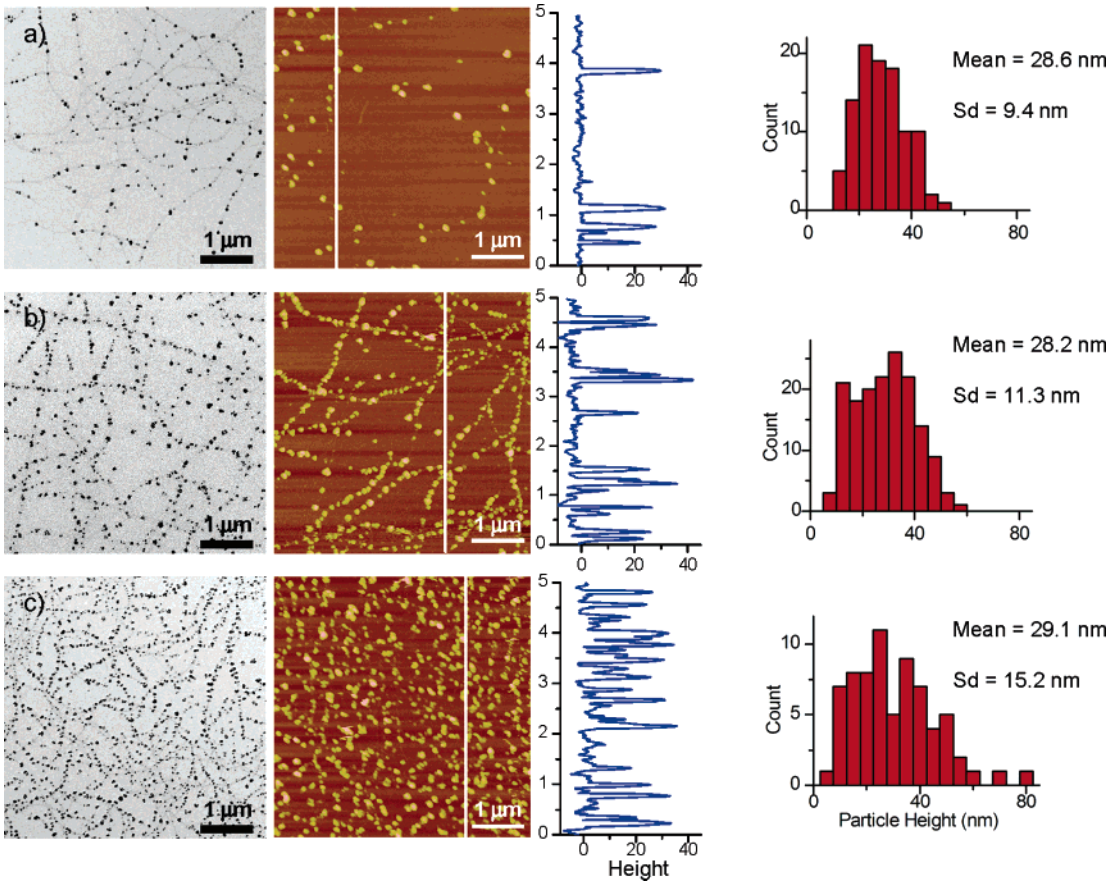


***Figure 7.*** FE-SEM images (first column) and AFM images (second column) of Ag nanoparticle growth at three high-density SWNT network electrodes (device 2). For all cases, the solution contained 1 mM $AgNO_3$ in 0.2 M $KNO_3$ and the potential was stepped from 0.0 to −1.0 V for (a) 200 ms, (b) 500 ms, and (c) 3 s. The white vertical lines in the AFM images denote the areas over which the cross-sectional line scans (third column) have been taken. Histogram analysis of particle heights for all three samples is also shown (fourth column).

The $i-t$ responses at −0.2 and −1.0 V (Figure 8a) are consistent with the microscopy observations. The peak current maximum, which designates the transition from isolated to interacting particles (overlapping diffusion fields), occurs at a longer time (8 ms) at the lower driving force of −0.2 V, compared with 5 ms at −1.0 V (also consistent with Figure 6b). We can ascribe this to a slower rate of nucleation of Ag nanoparticles on SWNTs at the lower driving force of −0.2 V compared to −1.0 V, so that a longer time elapses before there is significant interaction of the diffusion fields from neighboring particles. Note also that the final current is lower at −0.2 V, because the reaction is not driven at a maximum diffusion-controlled rate.

It is evident from the data presented for Ag that one can simply control the number (i.e., the density) of relatively uniform-sized particles in dense SWNT networks via the deposition time and by controlling the flux, via the applied potential.

**2. Pt Deposition.** A typical current−time curve for the nucleation of Pt on device type 2 is shown in Figure 9 over a time period of 5 s. Deposition was induced by stepping the potential from 0.0 V (where there was no reaction) to −0.5 V, just into the apparent diffusion-limited region for Pt deposition (as evidenced by separate voltammetric measurements; see the Supporting Information). The observed current falls rapidly toward zero after the potential step, indicating very little Pt deposition at short times. There is then an induction period (ca. 200 ms) before the current begins to rise slowly over a period of about 4 s, eventually attaining a quasi-steady-state value of ca. 280 nA. This behavior indicates that the kinetics of Pt deposition on SWNTs is significantly slower than for Ag.

The rising portion of the current transient shows an approximate $t^2$ dependence, in reasonable agreement with the $t^{3/2}$ current dependence expected for progressive nucleation and growth of noninteracting particles on a planar surface.[32] The subsequent transition to a quasi-steady-state plateau can be attributed to the onset of interaction between the diffusion fields of neighboring particles. The particles are then fed by a diffusion field that is simply determined by the area of the device, which is sufficiently small for a quasi steady state to be established (equivalent to a band electrode of 20 $\mu$m by 400 $\mu$m).

Figure 10 shows typical AFM images of SWNT networks after deposition of Pt at −0.5 V for defined periods of (a) 0.5 s and (b) 5 s, on devices with similar SWNT densities. These results, and additional data at 30 s (not shown), demonstrate that the density of Pt particles slowly increases with time from 1.5 particles $\mu m^{-1}_{SWNT}$ (4.2 $\mu m_{SWNT}$ $\mu m^{-2}$) at 0.5 s to 2.2 particles $\mu m^{-1}_{SWNT}$ (3.9 $\mu m_{SWNT}$ $\mu m^{-2}$) at 5 s and finally 2.6 particles $\mu m^{-1}_{SWNT}$ (5.1 $\mu m_{SWNT}$ $\mu m^{-2}$) at 30 s. The histogram analysis of nanoparticle size (Figure 10) shows that both the mean and the standard deviation of the observed diameters also increase with deposition time. It should be noted that even at

(32) See for example: Matthijs, E.; Langerock, S.; Michailova, E.; Heerman, L. *J. Electroanal. Chem.* **2004**, *570*, 123 and references therein.

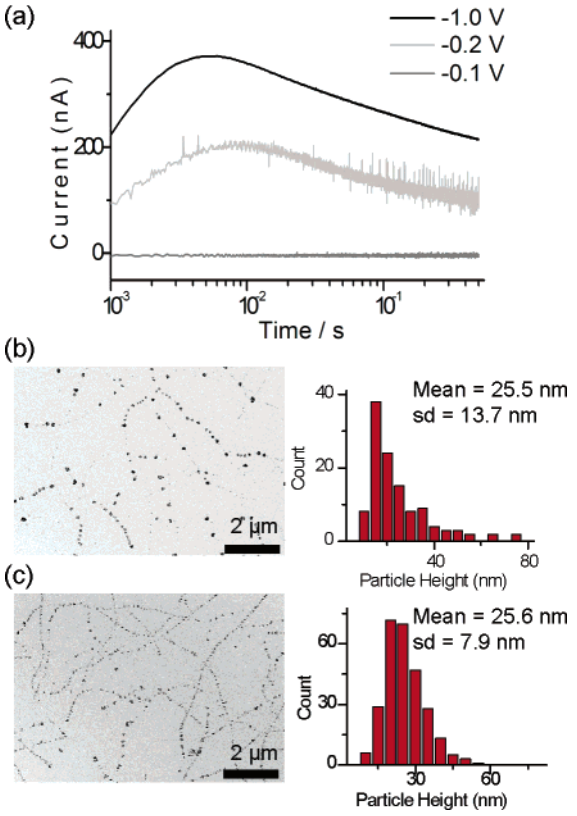


***Figure 8.*** (a) Current−time plots for the electrodeposition of Ag from a solution containing 1 mM $AgNO_3$ in 0.2 M $KNO_3$ at a high-density SWNT network electrode (device 2). The potential was stepped from 0.0 to −0.1 V (lower line), −0.2 V (middle line), and −1.0 V (upper line) on three different samples for a time period of 0.5 s. For −0.1 V no growth was observed using either FE-SEM or AFM. (b) and (c) are FE-SEM images for the −0.2 and −1.0 V deposition potential samples, respectively. The corresponding histogram analysis of particle heights for both samples is also shown.

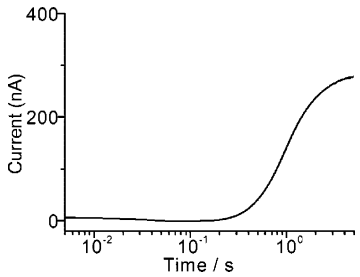


***Figure 9.*** Typical current−time curve for the nucleation of Pt on device type 2 (10 $\mu m_{SWNT}$ $\mu m^{-2}$) from a solution containing 2 mM $PtCl_6^{2-}$ and 0.5 M perchloric acid. Deposition was induced by stepping the potential from 0.0 to −0.5 V for 5 s.

0.5 s the AFM images demonstrate that most particles are within a distance of a few radii from each other, consistent with the transition to a quasi-steady-state current at about this time scale in the chronoamperometry experiments (Figure 9).

The electrical connectivity between the deposited metal nanoparticles and the underlying SWNTs was verified by recording the voltammetric characteristics for hydrogen adsorption/desorption and oxide formation in 0.5 M sulfuric acid at a Pt−SWNT composite electrode (produced by stepping the potential from 0.0 to −0.5 V for 30 s in a solution containing 2 mM $PtCl_6^{2-}$ in 0.5 M perchloric acid). Figure 11 shows the CV behavior at different scan rates in the range 0.5−10 V $s^{-1}$. Given that the average size of particles in this device was ca.

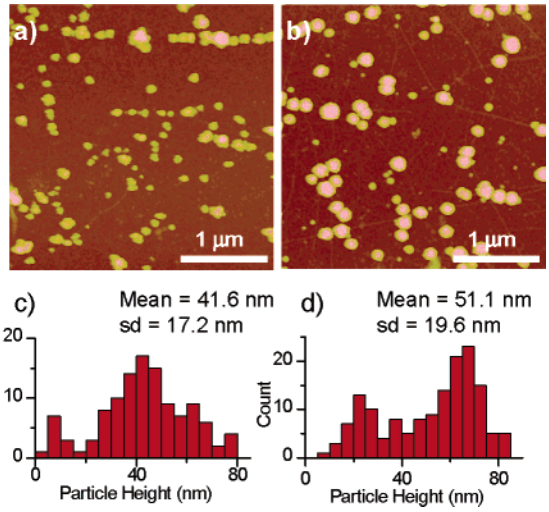


***Figure 10.*** AFM images of Pt nanoparticle growth at two high-density SWNT network electrodes (device 2). The solution contained 2 mM $PtCl_6^{2-}$ in 0.5 M perchloric acid, and the potential was stepped from 0.0 to −0.5 V for (a) 500 ms and (b) 5 s. Histogram analysis of particle heights for both samples is also shown (c, d).

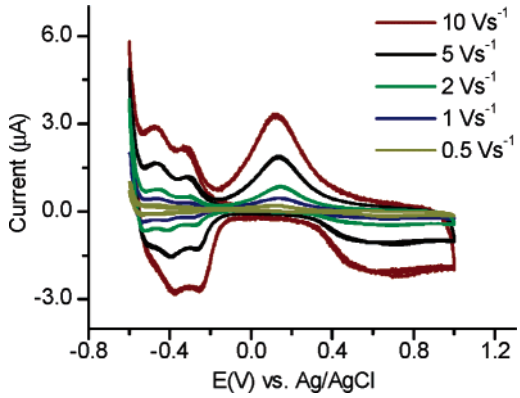


***Figure 11.*** Cyclic voltammograms for an SWNT−Pt composite electrode (device 2) in a solution containing 0.5 M $H_2SO_4$ at different scan rates in the range 0.5−10 V $s^{-1}$. Pt nanoparticles were nucleated from a solution containing 2 mM $PtCl_6^{2-}$ and 0.5 M perchloric acid onto the SWNT network by stepping the potential from 0.0 to −0.5 V for 30 s.

90 nm, the particles were large enough to exhibit a voltammetric signature characteristic of polycrystalline Pt.[33,34] In particular, it is clear that there are two pairs of hydrogen adsorption/desorption peaks in the potential range −0.2 to −0.4 V, attributed to the (111) and (100) Pt facets, together with a signature for oxide formation (more anodic than 0.4 V) and stripping (centered at 0.1 V). On devices which contained much smaller Pt particles the hydrogen adsorption/desorption waves became increasingly less discernible against the background signal.

Figures 6−10 demonstrate that, for both Ag and Pt, by careful choice of the applied potential and deposition time it is possible to control the density (and, especially for Ag, the size) of nanoparticles formed on electrodes consisting of networks of SWNTs. However, there are significant differences between the two metal deposition processes under the conditions employed. The studies reported above on device 2 demonstrate that the rate at which new particles are nucleated on SWNTs is much

(33) Ross, P. N. *J. Electrochem. Soc.* **1979**, *126*, 67.
(34) Zoval, J. V.; Lee, J.; Gorer, S.; Penner, R. M. *J. Phys. Chem. B* **1998**, *102*, 1166.

greater for Ag than for Pt. Furthermore, the Ag particles are typically more monodisperse than the Pt particles. For Ag, the growth system appears to be particularly monodisperse at shorter times (<500 ms).

A dominant factor in the metal particle nucleation rate will be the kinetics of electron transfer between the SWNTs and the metal ions in solution. The reduction of $Ag^+$ to Ag is a one-electron process, characterized by fast heterogeneous electron-transfer kinetics.[35] Under the driving conditions of our experiments, it is clear that Ag clusters readily form and grow on SWNTs, typically to a size of 25−30 nm. By comparison, our studies indicate that nucleation of Pt particles is slow and irreversible. Once nucleated, Pt nanoparticles grow at a significant rate compared to the nucleation rate of new particles on SWNTs, resulting in a lower density of larger particles for Pt compared with Ag.

## Conclusions

The studies described in this paper clearly demonstrate that SWNTs (grown on an insulating surface and electrically connected to a gold contact electrode) serve as a template for the electrodeposition of nanostructured metals (Ag and Pt) from aqueous solutions of metal salts. Using direct electrodeposition, it was possible to control the density and size of metal nanoparticles via the applied potential and time, while the corresponding amperometric signal (for potential step experiments) provided information on the underlying growth mechanism. In studies using an uninsulated gold contact exposed to solution, nanowires were observed to form near the contacts, with discrete nanoparticles forming further away, presenting a simple methodology for the production of electrically connected metal nanoparticles and nanowires on an insulating support. Furthermore, the current-carrying properties of nanowires formed in this way should be enhanced, given that the core contains a single SWNT, which can sustain current densities in excess of $10^9$ A $cm^{-2}$.[36]

Although Ag and Pt have been the subject of this paper, we expect interest in the use of SWNT networks to deposit other materials electrolytically, including conducting polymers and semiconductors. Given that the preparation of graded materials using in-plane potential gradients on thin film electrodes is currently attracting attention from several groups,[37] there would be scope for controlling the formation of such materials on SWNT networks. The effective potential gradient could be varied via the SWNT network density, the reaction rate (current flow), and/or the addition of a second contact electrode.

Although we focused intentionally on dense SWNT networks in which individual SWNTs were well-connected, it would also be of interest to study the behavior of low-density SWNT samples and individual SWNTs (where differences in the nucleation behavior of metallic versus semiconducting SWNTs could be elucidated)[20] using electrochemical approaches similar to those outlined in this paper.

**Acknowledgment.** We thank Steve York (Department of Physics) for help with FE-SEM. N.R.W. thanks the Leverhulme Trust (Grant F/00215/S) for a postdoctoral fellowship. J.V.M. thanks the Royal Society for a Research Fellowship and EPSRC for support (Grant GR/S24138/01).

**Supporting Information Available:** Low-magnification FE-SEM image of Ag deposition on an SWNT network electrode (device 2), cyclic voltammogram for Pt deposition onto an SWNT network electrode (device 2), and FE-SEM images, recorded in the same area at 1 and 10 kV, of Ag deposition on an SWNT network electrode (device 1). This material is available free of charge via the Internet at http://pubs.acs.org.

JA051320R

(35) Porter, J. D.; Robinson, T. O. *J. Phys. Chem.* **1993**, *97*, 6696.

(36) Yao, Z.; Kane, C. L.; Dekker: C.; *Phys. Rev. Lett.* **2000**, *84*, 2941.

(37) (a) Balss, K. M.; Coleman, B. D.; Lansford, C. H.; Haasch, R. T.; Bohn, P. M. *J. Phys. Chem. B* **2001**, *105*, 8970. (b) Sehayek, T.; Vaskevich, A.; Rubinstein, I. *J. Am. Chem. Soc.* **2003**, *125*, 4719. (c) Coleman, B. D.; Finnegan, N.; Bohn, P. M. *Thin Solid Films* **2004**, *467*, 121.